Damping of Superfluid Flow by a Thermal Cloud

R. Meppelink,[1] S. B. Koller,[1] J. M. Vogels,[1] H. T. C. Stoof,[2] and P. van der Straten[1]

[1]*Atom Optics and Ultrafast Dynamics, Utrecht University, Post Office Box 80,000, 3508 TA Utrecht, The Netherlands*

[2]*Institute for Theoretical Physics, Utrecht University, Post Office Box 80,000, 3508 TA Utrecht, The Netherlands*

(Received 4 September 2009; revised manuscript received 13 November 2009; published 23 December 2009)

One of the principal signatures of superfluidity is the frictionless flow of a superfluid through another substance. Here, we study the flow of a Bose-Einstein condensate through a thermal cloud and study its damping for different harmonic confinements and temperatures. The damping rates close to the collisionless regime are found to be in good agreement with Landau damping and become smaller for more homogeneous systems. In the hydrodynamic regime, we observe additional damping due to collisions, and we discuss the implications of these findings for superfluidity in this system.

DOI: 10.1103/PhysRevLett.103.265301 PACS numbers: 67.85.De, 03.75.Kk, 47.37.+q, 67.90.+z

In 1938, Kapitza, and independently Allen and Misener, discovered that liquid ^{4}He below the λ-point can flow almost frictionless. Kapitza named this behavior superfluidity [1,2]. Many of the properties of superfluid helium also appear in dilute Bose-Einstein condensation (BEC). The most striking signatures of superfluidity in BEC are quantized vortices [3,4], second sound [5], Josephson oscillations [6], and persistent flow [7]. In contrast to liquid helium, where the interatomic interaction is too strong to investigate the microscopic properties of superfluidity, the interactions in BEC are much weaker. The study of superfluid flow in dilute BECs can therefore deepen our understanding of superfluidity.

In this Letter, the flow of a BEC (the superfluid) through a thermal cloud is studied in a harmonic potential by exciting a dipole oscillation of the BEC, whereas the thermal cloud initially remains at rest. In the hydrodynamic regime, this out-of-phase mode of the trapped Bose gas is the analog of the usual second sound mode in bulk superfluid helium [8]. For this second sound dipole mode, we study for the first time its frequency and damping rate from the collisionless to the hydrodynamic regime. In contrast to liquid helium, our analysis allows for a direct measurement of the position of the superfluid component (condensed atoms) with respect to the normal fluid (thermal atoms), which allows for an unequivocal determination of the second sound dipole mode.

The thermal cloud can be tuned from the hydrodynamic regime into the collisionless regime, in which the mean-free path of the thermal atoms is larger than the axial size of the cloud. As we will show, the damping of the second sound dipole mode in a collisionless, partly condensed BEC is primarily caused by Landau damping; i.e., mean-field interactions mediate the transfer of energy from the condensate to the thermal cloud, leading to the damping of collective modes. Landau damping was first discussed by Landau in the context of the damping of plasma oscillations and plays a key role in a broad variety of fields, for instance the damping of phonons in metals, the damping of quarks and gluons in quark-gluon plasmas, and the anomalous skin effect in metals.

Previously, some experiments have been performed in which the BEC and the thermal cloud move with respect to each other [9,10]. In the latter experiment, the thermal cloud is in the collisionless regime. In the pioneering experiment [9], the thermal cloud is in the crossover region toward the hydrodynamic regime, but only one measurement series is presented. It therefore does not provide a study of the dependence of damping of the superfluid flow on, for instance, the temperature or the collision rate, which are the crucial parameters determining the damping rate. In contrast, the number of theoretical studies of this subject greatly outnumbers the available experimental work (see for instance Refs. [11–14]).

The experimental setup is capable of creating Bose-Einstein condensates containing up to 3×10^8 sodium atoms, limited by three-body decay [15]. In this setup, we have reached the axially hydrodynamic regime in the thermal cloud above the transition temperature T_c. The axially hydrodynamic regime is reached by evaporatively cooling atoms in an axially decompressed trap with an aspect ratio of up to 1:65 [16]. The radial trap frequency is given by $\omega_{\mathrm{rad}}/(2\pi) = 95.56$ Hz. Here, we cool atoms to temperatures below T_c for different values of the axial confinement.

A measure for the hydrodynamicity of the thermal cloud in the axial direction is $\tilde{\gamma} \equiv \gamma_{22}/\omega_{\mathrm{ax}}$, where the collision rate $\gamma_{22} = n_{\mathrm{eff}}\sigma v_{\mathrm{rel}}$ is the average number of collisions in the thermal cloud [17]. Here, v_{rel} is the relative velocity, $\sigma = 8\pi a^2$ is the isotropic cross section of two bosons with s-wave scattering length a, and $n_{\mathrm{eff}} = \int d\vec{r} n_{\mathrm{ex}}^2(\vec{r}) / \int d\vec{r} n_{\mathrm{ex}}(\vec{r})$ is the effective density of the trapped thermal atoms with density n_{ex}. For our parameters, $\gamma_{22} \simeq 90\ \mathrm{s}^{-1}$ for the highest number of atoms and weakest axial confinement, which corresponds to $\tilde{\gamma} \lesssim 10$. Note that the thermal cloud becomes less hydrodynamic for stronger axial confinement due to two effects: the increased three-body losses and the radial expansion. We

 © 2009 The American Physical Society

have observed the crossover from the collisionless to the hydrodynamic regime by studying the heat conduction in a thermal cloud above T_c [17]. Furthermore, the thermal cloud is deeper in the hydrodynamic regime when a BEC forms due to collisions with condensed atoms [12]. As a result, the thermal cloud is even more hydrodynamic below T_c than it is above the transition temperature.

The procedure used for the excitation of a second sound dipole mode, schematically shown in Fig. 1, is conducted as follows: initially, the center of the magnetic trap (MT) at $z = z_0$ [Fig. 1(a)] is displaced adiabatically in the axial direction over slightly more than the length of the BEC [Fig. 1(b)]. Next, a focused blue-detuned laser beam is aligned perpendicular to the axial axis of the system at position z_d with $z_0 < z_d < z_1$, where it does not overlap with the BEC [Fig. 1(c)]. This beam is detuned 25 nm below the ^{23}Na D_2 transition, and its intensity is gradually ramped up to roughly 10^4 mW/cm^2 in 100 ms. This corresponds to a maximum potential of roughly $V_{\mathrm{dip}} \simeq 1.1\mu$ with μ the chemical potential. The intensity is stabilized using a feedback circuit. Next, the center of the trap is displaced adiabatically back to its original position $z = z_0$ [Fig. 1(d)]. Since $\mu < V_{\mathrm{dip}} < k_B T$, with k_B the Boltzmann constant and T the temperature, only the thermal cloud can pass the dipole potential and return to $z = z_0$, while the condensate remains at $z = z_1$. Finally, the dipole beam is turned off, and the BEC will undergo a dipole oscillation, while the thermal cloud is initially at rest [Figs. 1(e) and 1(f)]. The distance $\Delta z = z_d - z_0$ determines the maximum velocity $v = \omega_{\mathrm{ax}} \Delta z$ of the center-of-mass of the condensate. The final position of the center of the MT is used to tune Δz and thus v.

We have excited the cloud for various v in order to observe whether there is a threshold velocity v_c above which the out-of-phase oscillation is strongly damped. The damping rate for different values of v is shown in Fig. 2. For $v > c$, we observe an increase of the damping rate of the out-of-phase oscillation for increasing v. The strong damping in this regime is accompanied by a large reduction of the condensate fraction, which eventually leads to the complete depletion of the BEC. For excitations with $v \lesssim v_c$, we observe a low damping rate, independent of v within the experimental accuracy. The threshold value depends on our trap geometry and is determined at $v_c/c \approx 0.59 \pm 0.05$ for the weakest axial confinement. For the strongest confinement used, we find $v_c/c \approx 0.8 \pm 0.1$. The observation of a threshold velocity indicates the onset of a strong damping mechanism, which we consider as the breakdown of superfluidity. The experiments described in the remainder of this Letter are conducted in the regime of low damping ($v < v_c$).

A measurement series contains ~100 shots at various hold time τ after the dipole beam is turned off. At the end of the hold time, an absorption image is taken after the cloud is allowed to expand during a 85 ms time-of-flight. During a measurement series, the situation before the dipole beam is turned off is monitored a few times to check for the absence of condensed atoms in the center of the trap. The thermal cloud is easily distinguished from the BEC in the absorption images due to the distinct density profiles. The final images are fitted to a bimodal distribution, which is the sum of a Maxwell-Bose distribution modeling the thermal cloud and a Thomas-Fermi (TF) distribution modeling the BEC. The fit yields ten parameters: the axial and radial positions, the axial and radial sizes, and the optical densities of both components. The axial position of both components is used to observe the dipole oscillations, the total absorption is used to determine the column density of both components, and the radial size of the thermal cloud is used to determine the temperature of the system. Furthermore, the aspect ratio of the condensate is used to detect the quadrupole oscillation induced by the excitation procedure, which turns out to be small, does not couple to the dipole mode, and is therefore not of interest.

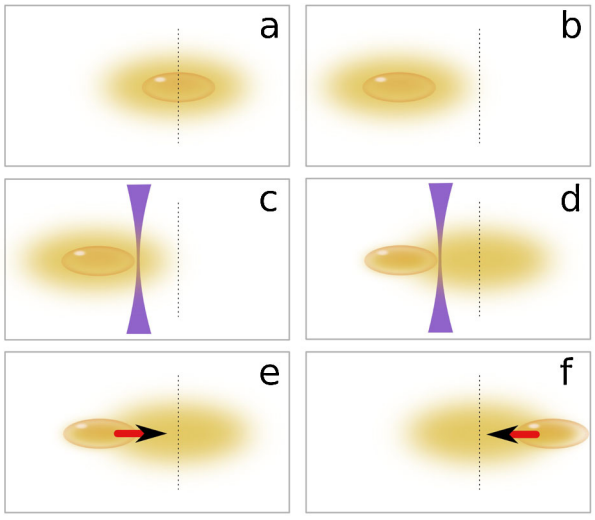

FIG. 1 (color online). Schematic representation of the excitation procedure of the second sound dipole oscillation. See text for more details.

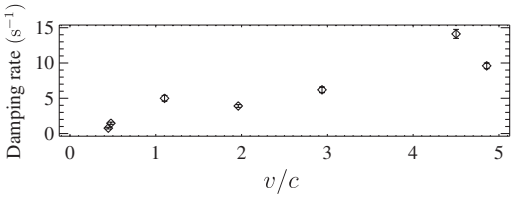

FIG. 2. The damping rate of the out-of-phase oscillation for $\omega_{\mathrm{ax}}/(2\pi) = 1.47$ Hz as a function of the initial velocity v/c, where $c = \sqrt{\mu/m}$ is the central speed of sound, μ the chemical potential determined using the measured BEC density, and m the mass. The uncertainty in the measured damping rate and in c is larger for high v due to the depletion of the condensate.

A series is measured for three values of the axial confinement and for two temperatures. To compare the results under these different conditions, the temperature is adjusted in such a way that for a given temperature, the initial chemical potential is roughly the same in all confinements. The axial position of the thermal cloud z_{ex} and the BEC z_{BEC} are plotted as a function of τ in Fig. 3. Furthermore, the difference $\Delta z = z_{BEC} - z_{ex}$ is plotted to isolate the out-of-phase dipole oscillation from the in-phase oscillation. The thermal cloud, initially at rest, starts to oscillate when the BEC moves through it, and eventually both clouds oscillate simultaneously and in-phase, as can be seen in Fig. 3. We refer to this final motion as the in-phase dipole oscillation. We have checked that the thermal cloud remains at rest as long as the dipole beam is present.

The positions z_{ex} and z_{BEC} are simultaneously fitted to a combination of two exponentially damped sinusoidal functions. The fit of the data yields the damping rate Γ_{ip} (Γ_{oop}) and the frequency ω_{ip} (ω_{oop}) of the in-phase (out-of-phase) dipole oscillation. The damping rate of the in-phase oscillation does not deviate from zero within the experimental uncertainty, as is expected for a harmonic trap. The axial trap frequency determined from the in-phase oscillation gives the same result as the trap frequency determination from a mutual center-of-mass oscillation ($\omega_{ip} = \omega_{ax}$). The quantities Γ_{oop} and ω_{oop} are plotted as a function of the trap frequency in Fig. 4.

In Fig. 4(a), one can see that Γ_{oop} decreases for decreasing axial trap frequency. However, Γ_{oop}/ω_{ax} increases for decreasing axial trap frequency as one can see in Fig. 4(b). This indicates that an extra damping mechanism independent on the trap frequency plays a significant role as well, especially for the highest T and thus the most hydrodynamic clouds.

The normalized second sound oscillation frequency ω_{oop}/ω_{ax} is shown in Fig. 4(c). For all conditions $\omega_{oop} < \omega_{ax}$, where under the most hydrodynamic conditions $\omega_{oop} \approx 0.94\omega_{ax}$. Furthermore, the largest deviations of ω_{oop}/ω_{ax} from 1 coincides with the largest Γ_{oop} and is found for the most hydrodynamic clouds. The shift of ω_{oop} with respect to ω_{ax}, up to 6% in our experiment, is larger than the shift of 4.5% observed in Ref. [9] and similar to the 6% shift reported in Ref. [10], although the reduced temperature T/T_c is lower in our experiments.

The mean-field potential of the thermal cloud causes the effective axial trapping potential to be slightly smaller. This effect reduces the effective trap frequency with $\sim$2% for the highest thermal density and cannot account for the shifts of up to 6%. As a consequence, the measured frequency shift and damping rate of the out-of-phase dipole mode both reflect that collisional effects play a role. Since ω_{oop} and ω_{ax} are determined simultaneously and with a high accuracy, the frequency shift gives an accurate measure for these effects.

As far as we know, there exists no theory that predicts the damping rate of a BEC by the thermal cloud in a trap from the collisionless to the hydrodynamic limit. Therefore, we compare the measured damping rates in Fig. 5 to Landau damping. Landau damping in a homogeneous, weakly interacting Bose gas has been described in the collisionless limit by several authors [18,19]. Landau damping increases with temperature because of the larger number of particle-hole pairs available at thermal equilibrium [20]. In our case, due to the confinement, both the

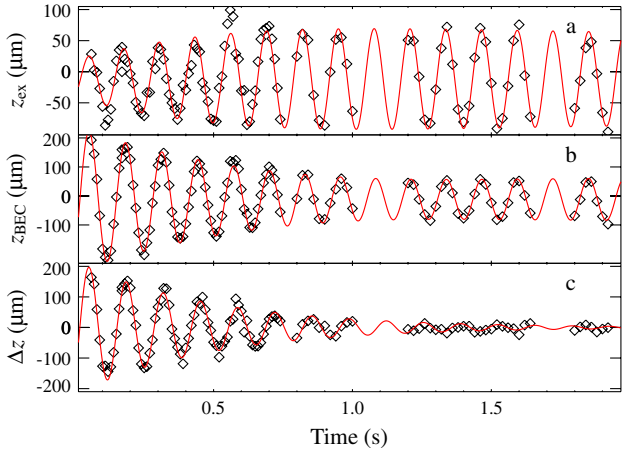

FIG. 3 (color online). The in-phase and out-of-phase dipole oscillation of a system characterized by $T = 0.39$ μK and $\mu/h = 2.6$ kHz for $\omega_{ax}/(2\pi) = 7.78$ Hz. In Figs. (a) and (b), the axial position z_{ex} of the thermal cloud and z_{BEC} of the BEC is plotted as a function of the hold time τ. In Fig. (c), the motion of the out-of-phase dipole oscillation is isolated by plotting Δz as a function of τ. The solid lines are the result of a fit to the data. Because of the destructive imaging scheme used, each point represents the position of a newly prepared cloud.

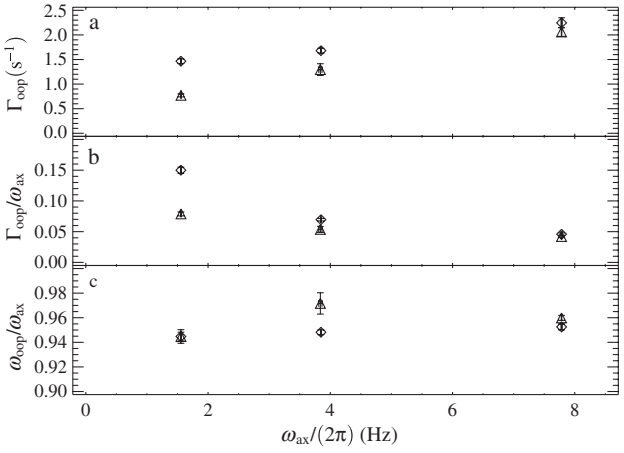

FIG. 4. The damping rate Γ_{oop} (a), the normalized damping rate Γ_{oop}/ω_{ax} (b), and the normalized frequency ω_{oop}/ω_{ax} (c) as a function of the axial trap frequency $\omega_{ax}/(2\pi)$. The chemical potential is $\mu \approx 0.4$ μK and the diamonds indicate the high temperature range ($\approx$0.5 μK), whereas the triangles indicate the low temperature range ($\approx$0.4 μK).

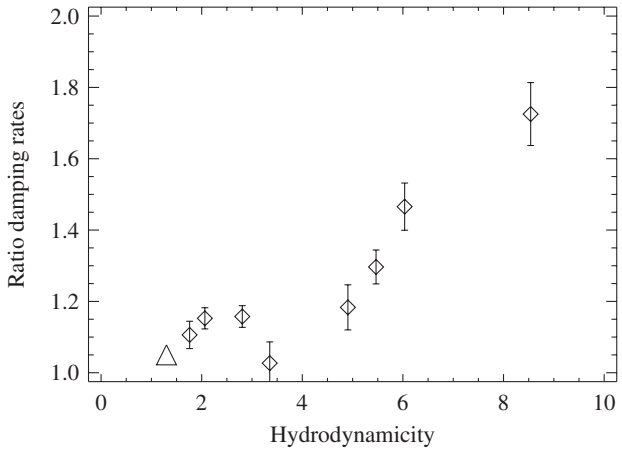

FIG. 5. The ratio of the measured damping rate and Landau damping $\Gamma_{\rm oop}/\Gamma_{\rm L}$ as a function of the hydrodynamicity parameter $\tilde{\gamma}$. The data point represented by the triangle is the result of a measurement taken from Ref. [9].

BEC and the thermal cloud have an inhomogeneous density distribution. Landau damping in such a system is determined by the condensate boundary region, and the result for the damping rate is different from that in a spatially homogeneous gas [21–23]. The damping rate for an inhomogeneous gas is given by $\Gamma_{\rm L} = \mathcal{C}\Gamma_{\rm Lh} = \mathcal{C}3\pi k_B T a\omega/(8\hbar c)$, where the speed of sound is given by $c = \sqrt{\mu/m}$ [23]. Furthermore, ω is the frequency of the excitation, $\Gamma_{\rm Lh}$ is the Landau damping rate for a homogeneous gas, and $\mathcal{C} = 12cm/\{\pi^{3/2}k_B\sqrt{m\hbar\omega}\log[2c^2m/(\hbar\omega)]\}$ is a numerical coefficient to incorporate the inhomogeneity [23]. Note that in our experiment, $\Gamma_{\rm L}$ is roughly independent of the speed of sound, since μ, and therefore the central density is roughly constant in the different confinements.

Figure 5 shows that we have measured the damping rate of the second sound dipole mode in a range from close to the collisionless up to the hydrodynamic regime with $\tilde{\gamma} \sim 10$. The ratio $\Gamma_{\rm oop}/\Gamma_{\rm L}$ increases strongly as a function of $\tilde{\gamma}$, and this may serve as a stringent test for theoretical models, which attempt to describe the damping of hydrodynamic excitations in the Landau two-fluid model. It shows that collisional processes, which have not been incorporated in the descriptions of Landau damping discussed above, play an important role in damping the second sound dipole mode.

In conclusion, we have measured the damping of the second sound dipole mode as a function of the axial confinement and the temperature. The damping raises interesting new insights in the frictionless flow of a superfluid through its thermal cloud. Our results in the collisionless regime corroborate the rates calculated for Landau damping, which shows that the rate decreases for decreasing excitation frequency. For a more homogeneous trap, this frequency goes down, and thus the damping rate will be smaller leading to frictionless flow for homogeneous systems. In the hydrodynamic regime, Landau damping is no longer dominant, and our results show that in this regime, the damping rate is strongly enhanced compared to the collisionless regime. Whether this collisional damping will also vanish for homogeneous systems remains an open question, which we hope will stimulate the development of new theoretical models to describe damping in the two-fluid model in the hydrodynamic regime.

This work is supported by the Stichting voor Fundamenteel Onderzoek der Materie ''FOM'' and by the Nederlandse Organisatie voor Wetenschaplijk Onderzoek ''NWO.''

[1] P. L. Kapitza, Nature (London) **141**, 74 (1938).
[2] J. F. Allen and A. D. Misener, Nature (London) **141**, 75 (1938).
[3] K. W. Madison, F. Chevy, W. Wohlleben, and J. Dalibard, Phys. Rev. Lett. **84**, 806 (2000).
[4] M. R. Matthews *et al.*, Phys. Rev. Lett. **83**, 2498 (1999).
[5] R. Meppelink, S. Koller, and P. van der Straten, Phys. Rev. A **80**, 043605 (2009).
[6] M. Albiez *et al.*, Phys. Rev. Lett. **95**, 010402 (2005).
[7] C. Ryu *et al.*, Phys. Rev. Lett. **99**, 260401 (2007).
[8] E. Zaremba, A. Griffin, and T. Nikuni, Phys. Rev. A **57**, 4695 (1998).
[9] D. M. Stamper-Kurn, H.-J. Miesner, S. Inouye, M. R. Andrews, and W. Ketterle, Phys. Rev. Lett. **81**, 500 (1998).
[10] F. Ferlaino *et al.*, Phys. Rev. A **66**, 011604(R) (2002).
[11] U. Al Khawaja and H. T. C. Stoof, Phys. Rev. A **62**, 053602 (2000).
[12] T. Nikuni and A. Griffin, Phys. Rev. A **65**, 011601(R) (2001).
[13] E. Zaremba, T. Nikuni, and A. Griffin, J. Low Temp. Phys. **116**, 277 (1999).
[14] E. Taylor and A. Griffin, Phys. Rev. A **72**, 053630 (2005).
[15] K. M. R. van der Stam, E. D. van Ooijen, R. Meppelink, J. M. Vogels, and P. van der Straten, Rev. Sci. Instrum. **78**, 013102 (2007).
[16] K. M. R. van der Stam, R. Meppelink, J. M. Vogels, and P. van der Straten, Phys. Rev. A **75**, 031602(R) (2007).
[17] R. Meppelink, R. van Rooij, J. M. Vogels, and P. van der Straten, Phys. Rev. Lett. **103**, 095301 (2009).
[18] P. C. Hohenberg and P. C. Martin, Ann. Phys. (N.Y.) **34**, 291 (1965).
[19] P. Szépfalusy and I. Kondor, Ann. Phys. (N.Y.) **82**, 1 (1974).
[20] F. Dalfovo, S. Giorgini, L. P. Pitaevskii, and S. Stringari, Rev. Mod. Phys. **71**, 463 (1999).
[21] W. Vincent Liu, Phys. Rev. Lett. **79**, 4056 (1997).
[22] L. P. Pitaevskii and S. Stringari, Phys. Lett. A **235**, 398 (1997).
[23] P. O. Fedichev, G. V. Shlyapnikov, and J. T. M. Walraven, Phys. Rev. Lett. **80**, 2269 (1998).